

Bloch Equation Enables Physics-informed Neural Network in Parametric Magnetic Resonance Imaging

Qingrui Cai^{1,3}, Liuhong Zhu², Jianjun Zhou^{2,3}, Chen Qian³, Di Guo⁴, and Xiaobo Qu^{1,3}

¹National Integrated Circuit Industry Education Integration Innovation Platform, School of Electronic Science and Engineering (National Model Microelectronics College), Xiamen University, Xiamen 361102, China

²Department of Radiology, Zhongshan Hospital (Xiamen), Fudan University, Xiamen 361015, China

³Department of Electronic Science, Fujian Provincial Key Laboratory of Plasma and Magnetic Resonance, Xiamen University, Xiamen 361102, China

⁴School of Computer and Information Engineering, Fujian Engineering Research Center for Medical Data Mining and Application, Xiamen University of Technology, Xiamen 361024, China.

Abstract—Magnetic resonance imaging (MRI) is an important non-invasive imaging method in clinical diagnosis. Beyond the common image structures, parametric imaging can provide the intrinsic tissue property thus could be used in quantitative evaluation. The emerging deep learning approach provides fast and accurate parameter estimation but still encounters the lack of network interpretation and enough training data. Even with a large amount of training data, the mismatch between the training and target data may introduce errors. Here, we propose one way that solely relies on the target scanned data and does not need a pre-defined training database. We provide a proof-of-concept that embeds the physical rule of MRI, the Bloch equation, into the loss of physics-informed neural network (PINN). PINN enables learning the Bloch equation, estimating the T_2 parameter, and generating a series of physically synthetic data. Experimental results are conducted on phantom and cardiac imaging to demonstrate its potential in quantitative MRI.

Keywords—Physics-informed neural network, deep learning, parametric imaging, Bloch equation, magnetic resonance imaging

I. INTRODUCTION

Quantitative magnetic resonance imaging (qMRI) can measure parameters that reflect the intrinsic characteristics of tissues [1]. Common quantitative parameters include T_1 , T_2 , T_2^* , extracellular volume fraction, etc.. T_1 , T_2 , T_2^* and myocardial extracellular volume fraction can be used to detect diffuse fibrosis [3], evaluate the degree of myocardial edema [4], quantifies tissue iron content [5], and reflects the degree of myocardial fibrosis [5], respectively. For example, T_1 and T_2 parameters (Fig. 1) could assess the histopathological changes of the myocardium and save the myocardium as early as possible [2].

Accurate parameter estimation is important. The estimation include two steps: First, solve the parametric signal model following the physical rule, Bloch equation, of MRI; Second, estimate parameters through fitting the signal model [6]. Thus, parameter estimation may encounter problems if the analytical solution is hard to be obtained [7]. On the other hand, advanced deep learning methods have shown great potential in qMRI [8], but deep learning methods usually lack interpretability and require a large amount of high-quality training labels [9].

Recently, to avoid using the pre-defined training database, physics-informed neural networks (PINN) [10-11] uses known physical equations as prior information and embeds them into the network's loss function.

In this work, we propose a PINN-based method for T_2 mapping in this work. We designed a physics-informed loss function that embeds the Bloch equation in PINN. By learning the Bloch equation through the network, it can obtain quantitative T_2 values by directly solving the inverse problem of equations without signal analytical formula and with only a single sample data. Once the PINN is trained, it can be used to generate physically synthetic MRI data.

II. PROPOSED METHOD

A. Bloch Equation

The magnetization vector $\mathbf{M} = (M_x, M_y, M_z)^T$ in the magnetic field satisfies the Bloch equation:

$$\frac{d\mathbf{M}(\mathbf{r}, t)}{dt} = \gamma \mathbf{M}(\mathbf{r}, t) \times \mathbf{B}(\mathbf{r}, t) - \frac{M_x(\mathbf{r}, t)\mathbf{i} + M_y(\mathbf{r}, t)\mathbf{j}}{T_2} - \frac{M_z(\mathbf{r}, t) - M_0}{T_1} \mathbf{k}, \quad (1)$$

where $\mathbf{B}(\mathbf{r}, t)$ is magnetic field at a spatial location \mathbf{r} , M_0 , T_1 , T_2 are tissue parameters. Due to the limitations of coil placement, in practical applications, the magnetization intensity M_z in the z-direction is difficult to be directly detected. Therefore, our target is the transverse magnetization vector $M_\perp = \sqrt{M_x^2 + M_y^2}$. For the multi-spin echo sequence (Fig. 2) that measures the T_2 value of tissues, the transverse magnetization vector M_\perp satisfies the Bloch equation that can be simplified as:

$$\frac{dM_\perp(\mathbf{r}, t)}{dt} + \frac{M_\perp(\mathbf{r}, t)}{T_2} = 0. \quad (2)$$

B. PINN for T_2 Mapping

Traditional quantitative T_2 mapping for a single voxel (without variable \mathbf{r}) uses the least square (Fig. 1).

According to Bloch equation (2), the signal analysis formula can be obtained:

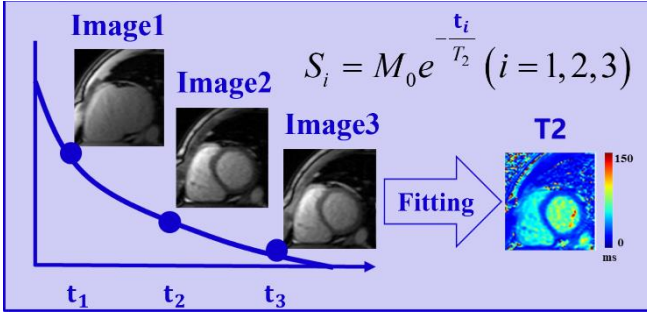


Fig. 1. Principle of least square for T_2 mapping.

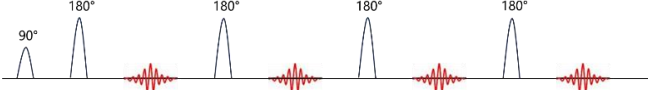


Fig. 2. Multi-spin echo sequence.

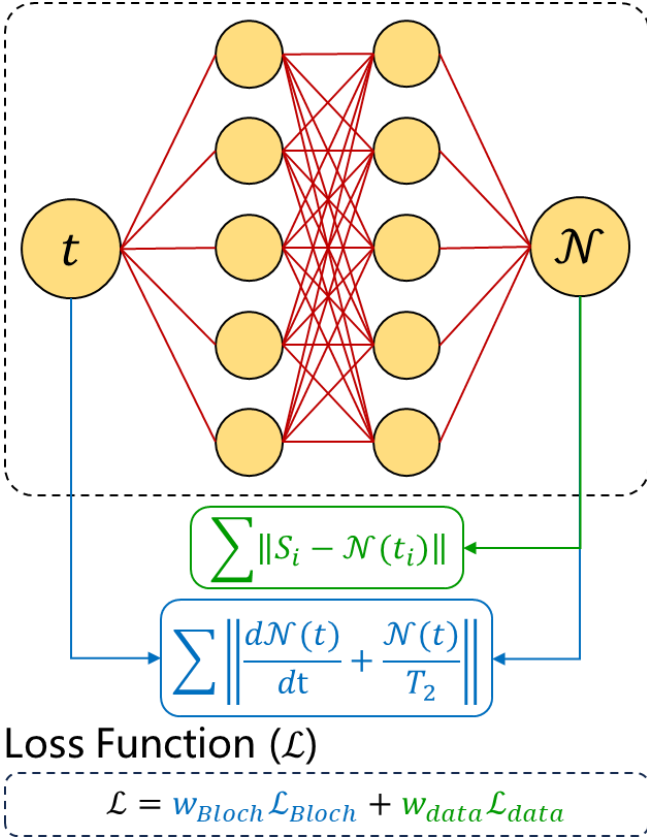


Fig. 3. Network structure of the Bloch equation-based PINN.

$$M_{\perp}(t) = M_0 e^{-\frac{t}{T_2}}, \quad (3)$$

where M_0 and T_2 are parameters to be quantified. For the measured data $M_{\perp}(t_i)$ in multiple time moments t_i , where $i \in \{1, 2, \dots, I\}$, I is the number of different contrast images, we set $M_{\perp}(t_i)$ as S_i . According to the signal analysis formula, we can obtain M_0 and T_2 through fitting with least square.

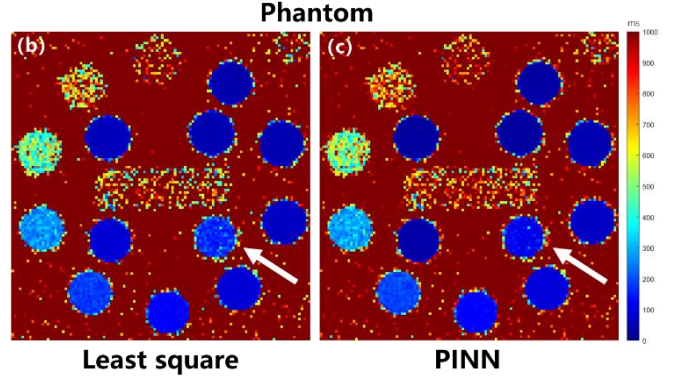
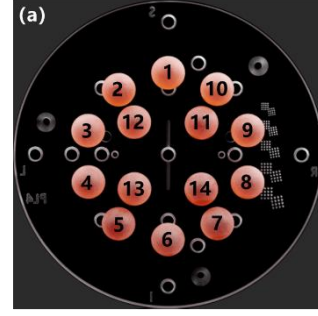


Fig. 4. T_2 mapping of $MnCl_2$ phantom. (a) An photo of the phantom, (b) and (c) are estimated T_2 values using the convetional least square and the proposed Bloch equation-based PINN, respectively.

However, for some sequences, the signal analysis formula cannot be obtained from Bloch equation, thus we use a nonlinear network is to approximate Bloch equation and obtain the quantitative parameters.

Here, we take multi-spin echo sequence as an example for quantitative T_2 mapping. The aim of PINN we propose is to approximate M_{\perp} in Bloch equation (2) by network training. The structure of PINN is a fully connected network with two hidden layer (Fig. 3). The input of PINN is t , where t is a set of K discrete time points in T_2 parameter interval, the network output is $\mathcal{N}(t)$. $\mathcal{N}(t)$ and $M_{\perp}(t)$ should satisfy the same equation:

$$\frac{d\mathcal{N}(t)}{dt} + \frac{\mathcal{N}(t)}{T_2} = 0. \quad (4)$$

The loss function of PINN is divided into two parts. The first part is a physics-informed loss for the Bloch equation (4):

$$\mathcal{L}_{Bloch} = \frac{1}{K} \sum_{k=1}^K \left\| \left(\frac{d\mathcal{N}(t)}{dt} + \frac{\mathcal{N}(t)}{T_2} \right) \Big|_{t=t_k} \right\|, \quad (5)$$

where $\|\cdot\|$ is the l_2 norm, $k \in \{1, 2, \dots, K\}$. The second part is the loss between the network output and the measured realistic cardiac qMRI data as follows:

$$\mathcal{L}_{data} = \frac{1}{I} \sum_{i=1}^I \|S_i - \mathcal{N}(t_i)\|. \quad (6)$$

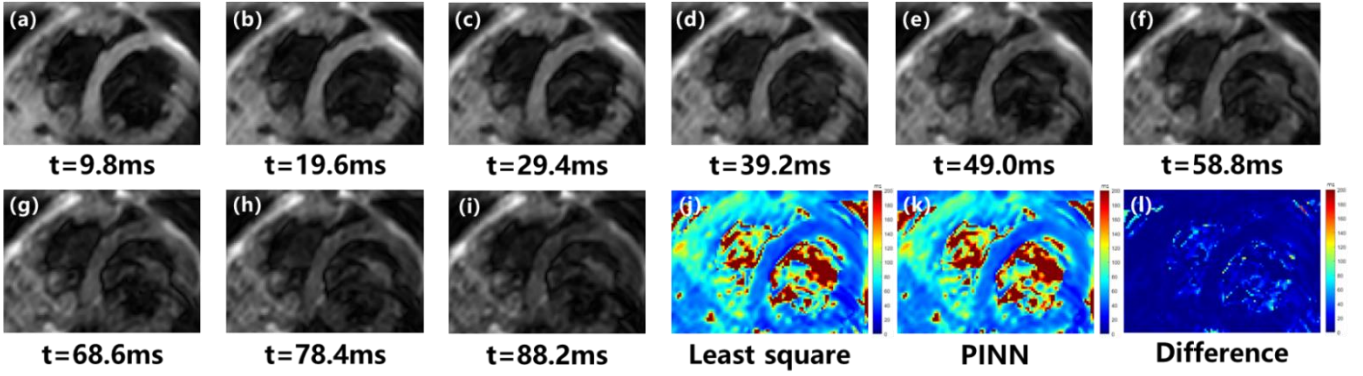


Fig. 5. T_2 mapping of cardiac MRI data from a healthy volunteer. (a)-(i) Nine different contrast images with different time t , (j) and (k) are estimated T_2 values using the conventional least square and the proposed Bloch equation-based PINN, respectively, (l) the difference between (j) and (k).

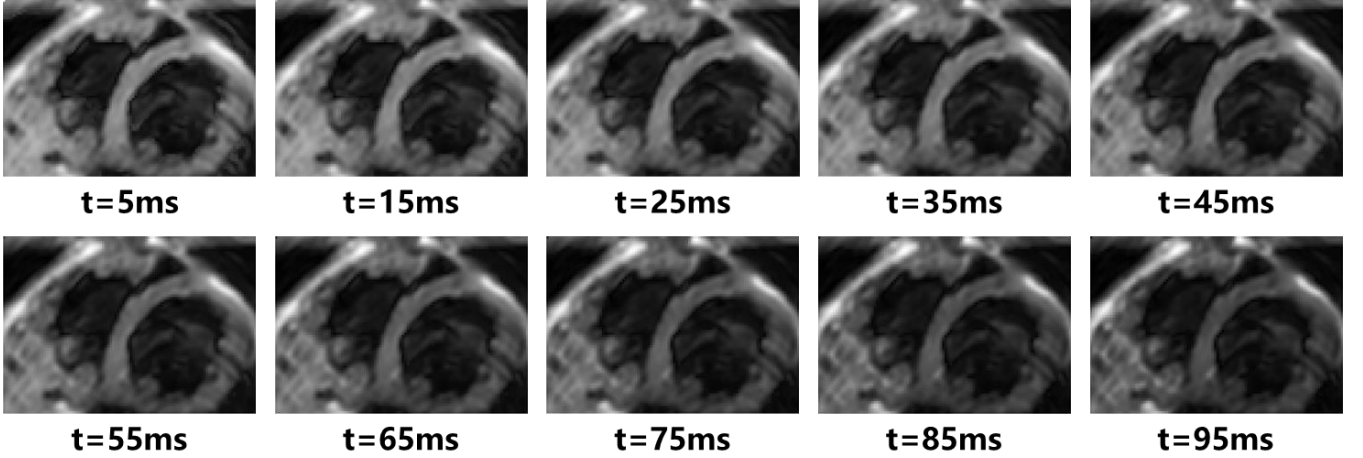


Fig. 6. Physically generated MRI data by using the PINN at different time t .

Finally, the total loss function is a weighted sum of two parts:

$$\mathcal{L} = w_{\text{Bloch}} \mathcal{L}_{\text{Bloch}} + w_{\text{data}} \mathcal{L}_{\text{data}}, \quad (7)$$

where w_{Bloch} and w_{data} are two weights to balance importance of two terms.

III. EXPERIMENTAL RESULT

A. Phantom

The phantom consists of 14 tubes that are filled with different concentrations of MnCl_2 solution (Fig. 4(a)) [12]. We acquired the imaging data on an United Imaging Healthcare 3.0T MRI scanner. Imaging parameters include $\text{FOV} = 240 \times 240 \text{ mm}^2$ and slice thickness = 2 mm. PINN parameters are $K = 1001$, $C = 8$, $w_{\text{Bloch}} = 0.01$, and $w_{\text{data}} = 1$.

Figs. 4(b) and (c) show that the estimated T_2 values by two approaches are close to each other at most tubes. For the tube #14 that have small T_2 value (The standard T_2 is 5.592 ms [12]), the estimated T_2 values by PINN is closer to the reported standard one than the conventional least square approach.

B. Healthy Volunteer

The cardiac imaging data were acquired from a healthy volunteer on a Philips 3.0T scanner. Imaging parameters are $\text{FOV} = 300 \times 300 \text{ mm}^2$ and slice thickness = 10 mm. PINN parameter include $K = 1001$, $C = 8$, $w_{\text{Bloch}} = 0.01$ and $w_{\text{data}} = 1$.

Given nine contrast images with different time t , the T_2 values estimated by two methods are comparable (Fig. 5).

C. Data Generation

The PINN approximates the relationship from time t to the transverse magnetization intensity $M_{\perp}(t)$ after training. Input time t , the corresponding transverse magnetization intensity $M_{\perp}(t)$ can be obtained for any voxel. Therefore, the trained PINN can be used to generate the MRI data at any time t (Fig. 6). This may benefit physics-driven deep learning, particularly when a large amount of training data is not available [9, 13-15].

IV. CONCLUSION

This paper proposes to incorporate the physical rule of MRI, the Bloch equation, into the neural network learning. No matter on phantom or realistic data, T_2 maps obtained for by two methods are comparable. Thus, the Bloch equation enables physics-informed neural network in parametric magnetic resonance imaging.

ACKNOWLEDGMENTS

This work was partially supported by the National Natural Science Foundation of China (62122064, 61971361, 62371410 and 62331021), the Natural Science Foundation of Fujian Province of China (2023J02005 and 2021J011184), the President Fund of Xiamen University (20720220063), and Nanqiang Outstanding Talent Program of Xiamen University. Thanks are due to Huajun She, Bei Liu and Wenlong Feng

from School of Biomedical Engineering, Shanghai Jiao Tong University for providing quantitative phantom data.

(*Corresponding author: Xiaobo Qu, Email: quxiaobo@xmu.edu.cn)

REFERENCES

- [1] X. Zhang, H. Lu, D. Guo, Z. Lai, H. Ye, X. Peng, et al., "Accelerated MRI reconstruction with separable and enhanced low-rank Hankel regularization," *IEEE Trans. Med. Imaging*, vol. 41, no. 9, pp. 2486-2498, 2022.
- [2] C. Tschöpe, E. Ammirati, B. Bozkurt, A. L. P. Caforio, L. T. Cooper, S. B. Felix, et al., "Myocarditis and inflammatory cardiomyopathy: Current evidence and future directions," *Nat. Rev. Cardiol.*, vol. 18, no. 3, pp. 169-193, 2021.
- [3] B. Yaman, S. Weingärtner, N. Kargas, N. D. Sidiropoulos, M. Akçakaya, "Low-rank tensor models for improved multidimensional MRI: Application to dynamic cardiac T1 mapping," *IEEE Trans. Comput. Imaging*, vol. 6, pp. 194-207, 2020.
- [4] B. Baessler, C. Luecke, J. Lurz, K. Klingel, A. Das, M. Roeder, et al., "Cardiac MRI and texture analysis of myocardial T1 and T2 maps in myocarditis with acute versus chronic symptoms of heart failure," *Radiology*, vol. 292, no. 3, pp. 608-617, 2019.
- [5] F. Cadour, J. Cautela, S. Rapacchi, A. Varoquaux, P. Habert, F. Arnaud, et al., "Cardiac MRI features and prognostic value in immune checkpoint inhibitor-induced myocarditis," *Radiology*, vol. 303, no. 3, pp. 512-521, 2022.
- [6] Y. Fatemi, H. Danyali, M. S. Helfroush, H. Amiri, "Fast T2 mapping using multi-echo spin-echo MRI: A linear order approach," *Magn. Reson. Med.*, vol. 84, no. 5, pp. 2815-2830, 2020.
- [7] C. Cai, Chao. Wang, Y. Zeng, S. Cai, D. Liang, Y. Wu, et al., "Single-shot T2 mapping using overlapping-echo detachment planar imaging and a deep convolutional neural network," *Magn. Reson. Med.*, vol. 80, no. 5, pp. 2202-2214, 2018.
- [8] Y. Li, Y. Wang, H. Qi, Z. Hu, Z. Chen, R. Yang, et al., "Deep learning-enhanced T1 mapping with spatial-temporal and physical constraint," *Magn. Reson. Med.*, vol. 86, no. 3, pp. 1647-1661, 2021.
- [9] Q. Yang, Z. Wang, K. Guo, C. Cai, X. Qu, "Physics-driven synthetic data learning for biomedical magnetic resonance: The imaging physics-based data synthesis paradigm for artificial intelligence," *IEEE Signal Process. Mag.*, vol. 40, no. 2, pp. 129-140, 2023.
- [10] M. Raissi, P. Perdikaris, G. E. Karniadakis, "Physics-informed neural networks: A deep learning framework for solving forward and inverse problems involving nonlinear partial differential equations," *J. Comput. Phys.*, vol. 378, pp. 686-707, 2019.
- [11] G. E. Karniadakis, I. G. Kevrekidis, L. Lu, P. Perdikaris, S. Wang, L. Yang, "Physics-informed machine learning," *Nat. Rev. Phys.*, vol. 3, no. 6, pp. 422-440, 2021.
- [12] <https://qmri.com/product/ismrm-nist-premium-system-phantom/>
- [13] C. Qian, Z. Wang, X. Zhang, Q. Cai, T. Kang, B. Jiang, et al., "Physics-informed deep diffusion MRI reconstruction: Break the bottleneck of training data in artificial intelligence," *2023 IEEE 20th International Symposium on Biomedical Imaging (ISBI)*, pp. 1-5, 2023.
- [14] Z. Wang, X. Yu, C. Wang, W. Chen, J. Wang, Y. Chu, et al., "One for multiple: Physics-informed synthetic data boosts generalizable deep learning for fast MRI reconstruction," arXiv preprint arXiv:2307.13220, 2023.
- [15] D. Chen, M. Lin, H. Liu, J. Li, Y. Zhou, T. Kang, et al., "Magnetic resonance spectroscopy quantification aided by deep estimations of imperfection factors and overall macromolecular signal," arXiv preprint arXiv:2306.09681, 2023.